

Blockage effects on aerodynamics and flutter performance of a streamlined box girder

Yongle Li^{*}, Junjie Guo^a, Xingyu Chen, Haojun Tang and Jingyu Zhang

Department of Bridge Engineering, Southwest Jiaotong University, Chengdu 610031, China

(Received March 12, 2019, Revised May 20, 2019, Accepted June 9, 2019)

Abstract. Wind tunnel test is one of the most important means to study the flutter performance of bridges, but there are blockage effects in flutter test due to the size limitation of the wind tunnel. On the other hand, the size of computational domain can be defined by users in the numerical simulation. This paper presents a study on blockage effects of a simplified box girder by computation fluid dynamics (CFD) simulation, the blockage effects on the aerodynamic characteristics and flutter performance of a long-span suspension bridge are studied. The results show that the aerodynamic coefficients and the absolute value of mean pressure coefficient increase with the increase of the blockage ratio. And the aerodynamic coefficients can be corrected by the mean wind speed in the plane of leading edge of model. At each angle of attack, the critical flutter wind speed decreases as the blockage ratio increases, but the difference is that bending-torsion coupled flutter and torsional flutter occur at lower and larger angles of attack respectively. Finally, the correction formula of critical wind speed at 0° angle of attack is given, which can provide reference for wind resistance design of streamlined box girders in practical engineering.

Keywords: blockage effects; flutter performance; numerical simulation; wind speed correction; streamlined box girder

1. Introduction

Wing flutter was discovered in the aviation industry long before the wind damage of the old Tacoma Bridge. Theodorsen (1935) proposed the equation of the self-excited force for an ideal flat plate, which can simulate the aerodynamic self-excited force of a thin wing section with complete streamlined shape. Scanlan (1971) extended the flutter derivative theory of aircraft to the bridge section. Based on this theory, the flutter derivative of bridge section can be extracted by wind tunnel test and CFD numerical simulation.

Wind tunnel test is one of the important means to study the flutter performance of bridges. It can simulate the real wind environment at the bridge site, so as to determine the aerodynamic characteristics of bridges and the characteristics of the surrounding flow field (Ge and Xiang, 2008). Streamlined box girder is an effective cross-section form with great torsional stiffness, structural stability and economic advantage (Larsen and Wall 2012, Ito *et al.* 2014, He *et al.* 2017). After more than half a century of development, streamlined box girder has become the mainstream choice of long-span bridge, and been widely adopted in long-span bridges around the world, such as Great Belt Suspension Bridge, Sutong Bridge, Xiangshan Harbor Bridge, etc. (Larsen 1993, Ma *et al.* 2018, Zhu *et al.* 2013). However, with the increasing spans being employed,

the flutter performance of the bridge becomes an important research hotspot in the design process. Larsen (1993) studied in detail the effects of aerodynamic components such as guardrail, deflector and wind fairing on critical flutter wind speed in a wind tunnel test of the Great Belt Bridge. Larsen *et al.* (2008) conducted a series of wind tunnel tests of sectional models with different scales and studied the aerodynamic characteristics of the Stonecutters Bridge. Ge *et al.* (2009) investigated the flutter stability of Xihoumen Bridge through wind tunnel test and theoretical analysis, and found that aerodynamic damping is the main factor affecting flutter stability. Sukamta *et al.* (2008) investigated the effects of a wind fairing on the flutter stability for a twin-box girder by wind tunnel tests.

The real bridge is constructed in the atmospheric flow field with no boundary, however, the wind tunnels are bounded by walls. The limited wind tunnel space to simulate the real atmosphere is bound to be accompanied by the interference of the tunnel wall, leading to differences in aerodynamic forces, flow fields and so on. Thus, the blockage effects are inevitable. In addition, the characteristics of bluff body of the bridge girder is more obvious at large angles of attack due to a relatively wide flow and wake (Gu and Huang 2016). The blockage effects are mainly measured by the model size and the section size of the wind tunnel test, and characterized by the blockage ratio. It is defined as the ratio of the orthographic projection area of the bridge model to the inlet area of the wind tunnel. It is generally believed that the blockage effects can be neglected by controlling the blockage ratio to less than 5% (Hunt 1982, Kubo *et al.* 1989). But Takeda and Kato (1992) believe that the effect of 5% blockage ratio on the test results is quite serious, and there is no reliable basis for this criterion. The reason for allowing the larger blockage ratio

*Corresponding author, Professor,
E-mail: lele@swjtu.edu.cn

^a Ph.D. candidate,
E-mail: gjunjie456@163.com

in wind tunnel test is to emphasize the relative comparison between different design schemes. However, the result of calculation must be corrected to get the accurate value of the test result. At present, blockage effects and its correction have been studied in many fields such as aerospace, automobile and building structure. Cheng (2003) found that in low-speed solid-wall wind tunnels, when the angle of attack approached to 90° , a blockage ratio of 6.6% would cause 25% error in the drag coefficient of the YF-16 aircraft model. Huang and Gu (2015) carried out the blockage effects test of high-rise buildings and a new correction formula for mean pressure of rectangular high-rise buildings in uniform flow was proposed based on the test results. Li *et al.* (2018) found that 5% blockage ratio would cause 23.2% error in the amplitude of vortex-induced vibration (VIV) for flat box girder. At present, there are still few studies on the blockage effects of bridge wind tunnel test. The blockage effects on flutter performance of bridge are still unclear, so it is necessary to study the blockage effects of flutter for streamlined box girder.

In addition to wind tunnel tests, CFD numerical simulation is also one of the important methods to study the flutter performance of bridges (Zhou *et al.* 2015). CFD simulation is not only repeatable, but also unaffected by the inherent constraints (wind tunnel wall interference, bracket interference, etc.). Walther (1994) applied the discrete vortex method to simulate the flow field around the main girder of the Great Belt East Bridge, and calculated the aerodynamic derivative by forced vibration method. Larsen (2000) clarified the flutter mechanism of Tacoma bridge based on the discrete vortex method. Zhu and Chen (2004) found that the critical flutter wind speed of the Great Belt East Bridge calculated by CFD numerical simulation and the wind tunnel test is consistent. Tang *et al.* (2018) calculated the flutter derivatives of a thin plate by CFD technique, which agree well with the theoretical solution obtained by Theodorsen, and verified the reliability of the CFD method.

In this study, the real cross section of bridge is simplified as an ideal box girder and different numerical models corresponding to multiple blockage ratios are established. At first, the blockage effects on aerodynamic characteristics of stationary cross sections are analyzed, including aerodynamic coefficients, mean pressure distributions and velocity near the girder. And the aerodynamic coefficients are corrected according to the mean wind speed in the plane of leading edge of the model. Then the flutter derivatives are extracted by forced vibration and the critical flutter states of a real long-span suspension bridge are analyzed at different blockage ratios. Subsequently, the flutter type is discussed from the perspective of the changes in dynamic flow field and input energy provided by pitching moment. Finally, the correction formula of the critical flutter wind speed of the streamlined box girder at 0° angle of attack is given and a reasonable range of blockage ratio is proposed, which can provide reference for wind resistance design of streamlined box girders in practical engineering.

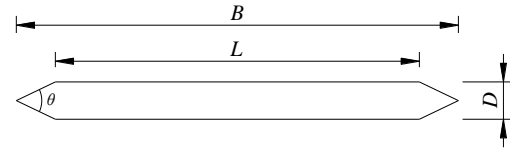


Fig. 1 Geometrical parameters of a streamlined box girder

2. CFD model

For the sectional model wind tunnel test, the longitudinal length of the bridge is equal to the width of the wind tunnel, so the blockage ratio is equal to the ratio of the orthographic projection height of the bridge model to the height of the wind tunnel, denoted by φ . Therefore, two-dimensional (2D) numerical models can be established to simulate the experimental conditions in the wind tunnel using CFD software. Fig. 1 shows the detailed geometric parameters of the streamlined box girder, such as the height of the streamlined box girder ($D = 0.1$ m), width of the girder without wind fairings ($L = 1$ m), width of the girder including wind fairings ($B = 1.2145$ m) and angle of wind fairing ($\theta = 50^\circ$).

The computational domain and boundary conditions utilized in this study are shown in Fig. 2. The length in the mean-flow direction is $30B$ and the upper and lower boundaries are set to wall to simulate wind tunnel walls. The height in the cross-flow direction of different models is set to $100D \sim 10D$, corresponding to the blockage ratio of 1%~10%, respectively. The windward side boundary $7.5B$ from the center of box girder is set as velocity-inlet, and the leeward side boundary $22.5B$ from the center of box girder is set as pressure-outlet. The boundary of the box girder is set as a smooth wall and its vertical symmetrical axis is located on the midline of the upper and lower boundaries. The streamlined box girder is rotated to achieve the changing of angle of attack. It is worth mentioning that the actual windshield height of the box girder should include the increased windshield height after rotation, so the real blockage ratios is greater than the corresponding aforementioned blockage ratios at positive angles of attack. The inlet wind velocity is uniform with a turbulence intensity of 0.5%, and the turbulence viscosity ratio is 2 (Huang *et al.* 2009). To balance calculation accuracy and computational efficiency, the computation domain is divided into three parts: rigid mesh zone, dynamic mesh zone and fixed mesh zone. The rigid mesh zone moves along with the box girder to ensure the quality of the mesh near the girder, which is discretized by quadrilateral unstructured grids. The dynamic mesh zone and the fixed mesh zone are discretized by triangular unstructured grids and quadrilateral structured grids, respectively. The element size progressively increases from the boundaries of the box girder to the computational boundaries, and the local computational mesh is shown in Fig. 3. In order to avoid errors of grid difference on the calculation results in different blockage ratios, the grids in the rigid mesh zone and the dynamic mesh zone keep the same, and there are only differences in the fixed mesh zone. The total number of meshes with different blockage ratios varies from 166805

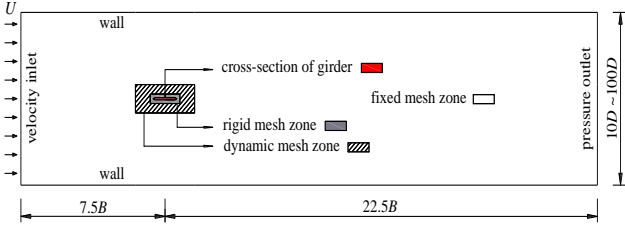


Fig. 2 Computational domain

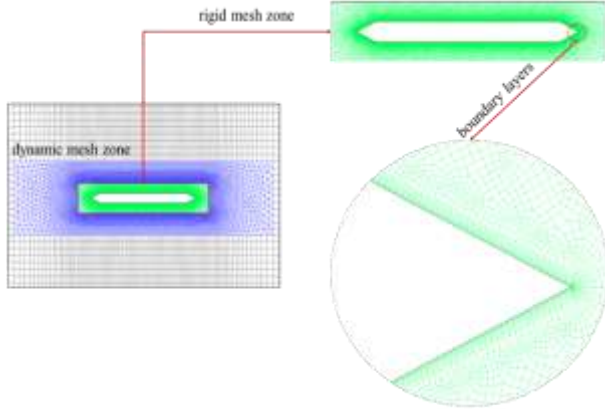


Fig. 3 Local computational mesh of CFD model

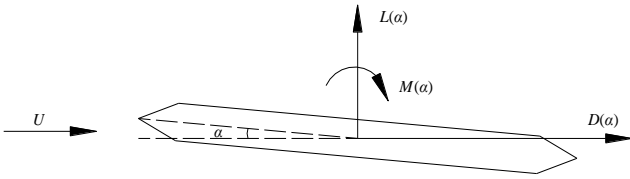


Fig. 4 Static forces acting on box girder

to 229235. RANS simulations are achieved by using the $k-\omega$ SST model which can make results more accurate than $k-\varepsilon$ model in external aerodynamic cases that involve boundary layer separation (Miranda *et al.* 2015).

The time-step is set to 0.001s. The discretized problem is numerically solved by using a SIMPLEC pressure-

velocity coupling algorithm. Momentum equation, turbulent kinetic energy equation and turbulent dissipation rate equation are all solved by second-order schemes. The CFD software FLUENT is utilized to simulate in this paper.

3. Blockage effects of aerodynamic characteristics of stationary cross section

3.1 Aerodynamic coefficients

The aerodynamic coefficients of the stationary box girder are first analyzed. The cross section of the box girder is subjected to drag force (down-wind), lift force (upward) and pitching moment (nose-up) in a fluid, which are represented by $D(\alpha)$, $L(\alpha)$ and $M(\alpha)$ respectively, as shown in Fig. 4. The drag, lift, and moment coefficients are defined as Eqs. (1)-(3)

$$C_D(\alpha) = D(\alpha)/(0.5\rho U^2 D) \quad (1)$$

$$C_L(\alpha) = L(\alpha)/(0.5\rho U^2 B) \quad (2)$$

$$C_M(\alpha) = M(\alpha)/(0.5\rho U^2 B^2) \quad (3)$$

where α is the angle of attack; ρ is the air density; B and D are the width and height of box girder respectively; U is the mean wind speed and set to 20 m/s; and the cases at 0° , $+5^\circ$ and $+10^\circ$ angles of attack are chosen for analysis in this part.

The mean aerodynamic coefficients of the streamlined box girder versus blockage ratio at three angles of attack are shown in Fig. 5. At 0° angle of attack, C_D increases gradually as the blockage ratio increases, while C_L and C_M are always close to zero. At $+5^\circ$ and $+10^\circ$ angles of attack, the larger the blockage ratio, the greater C_D , C_L and C_M . The effects of the blockage ratio on the aerodynamic coefficients become more apparent with the increase in angle of attack. At $+10^\circ$ angles of attack, taking the aerodynamic coefficients at 1% blockage ratio as the standard, C_D , C_L and C_M increase by 74.5%, 96.2% and 98.7% respectively when the blockage ratio increases to

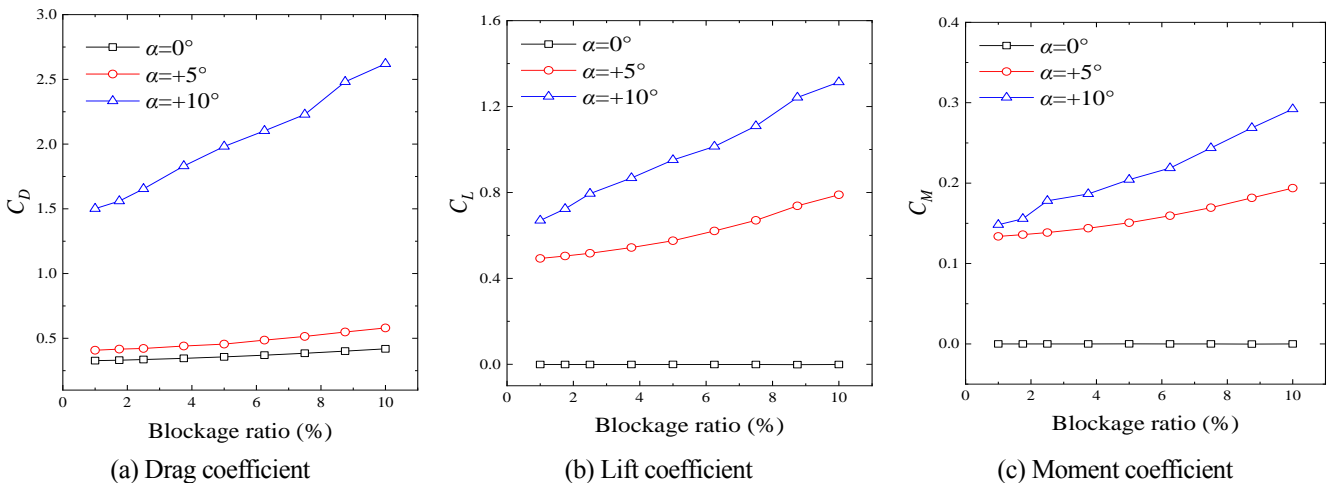


Fig. 5 Mean aerodynamic coefficients versus blockage ratio

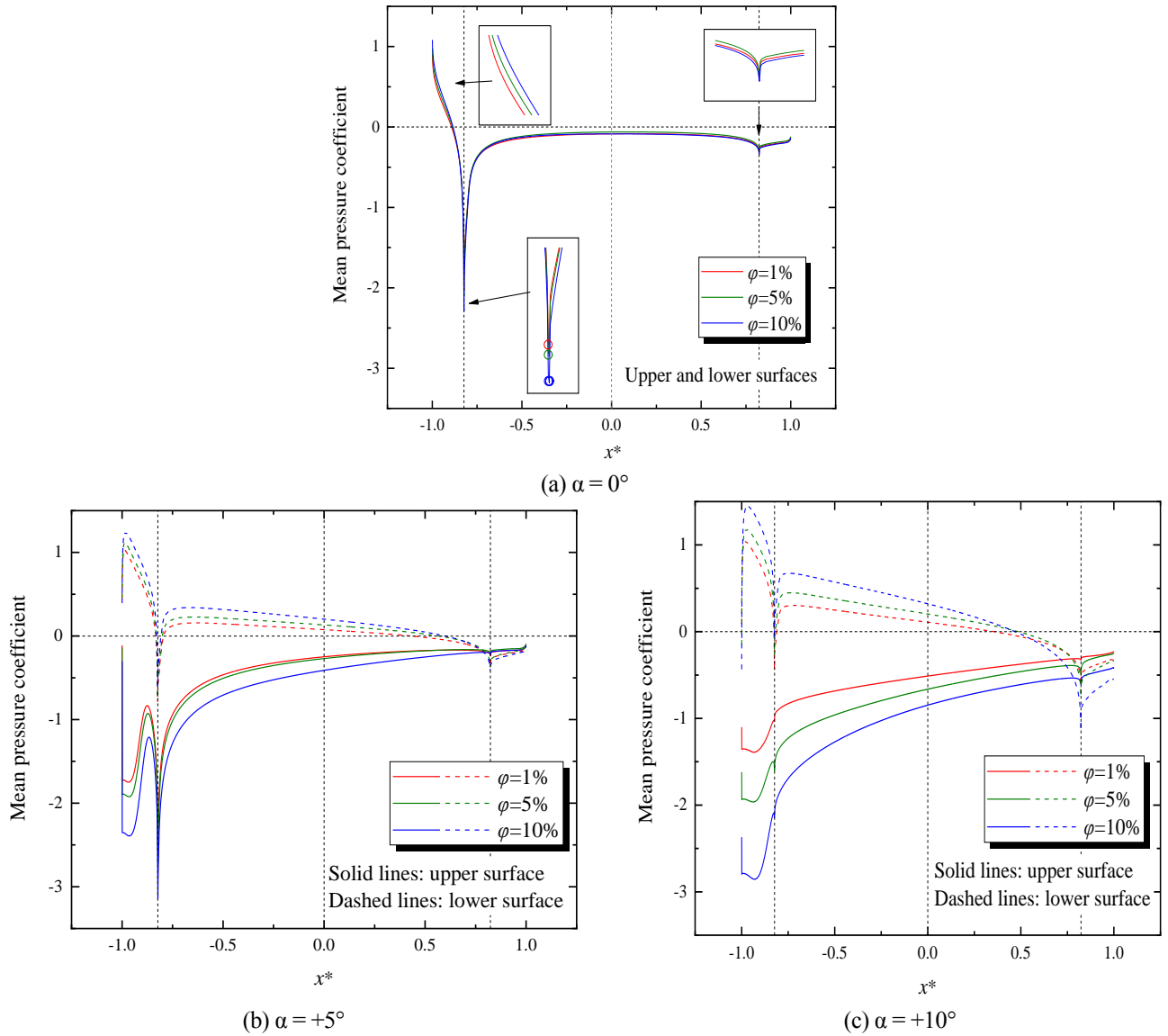


Fig. 6 Mean pressure distributions of the box girder for different blockage ratios

10%. In conclusion, the blockage effects on the aerodynamic coefficients are so obvious that it cannot be ignored. Thus, the blockage ratio should be reduced as far as possible when calculating and testing the aerodynamic coefficients of the bridge structures, especially at large angles of attack

3.2 Pressure distributions

Then the pressure distributions of the simplified box girder at different blockage ratios are analyzed. The mean pressures (\bar{p}) are normalized by the dynamic pressure ($0.5\rho U^2$) of flow, and the mean pressure coefficient can be expressed as $C\bar{p} = \bar{p}/0.5\rho U^2$. The dimensionless parameter x^* (normalized by $0.5B$) is the abscissa, and the variation range is from -1 to 1, representing different positions on the surface of the box girder, where -1, 0 and 1 represent the leading edge, the center and the trailing edge of the box girder respectively. Although the models are based on the wind axis coordinate system to simulate the

situation in the real wind tunnel, the pressure coefficients at positive angles of attack are expressed under the body axis coordinate system for convenience comparison. The wind velocity is still set to 20 m/s, Figs. 6 and 7 show the mean pressure coefficient distributions and the contours of static pressure of the stationary cross sections for different blockage ratios respectively.

At 0° angle of attack, the pressure distributions on the upper and lower surfaces are the same because the ideal box girder is vertically symmetrical, so C_L and C_M are approximately equal to 0. The box girder acts like a streamlined cross section, the incoming flow is separated at the tip of the wind fairing, the windward side is subjected to positive pressure, so the value of C_D is positive. The pressure at the tip of the upstream wind fairing is the largest, exceeding 100 Pa. The area around the wind fairing that exceeds 50 Pa expands as the blockage ratio increases, resulting in an increase in C_D . Observing Fig. 6(a), the blockage ratio has a limited effect on the mean pressure coefficient of the upper and lower surfaces. At the

windward end, $C\bar{p}$ changes its sign from positive to negative, showing a decreasing trend, and the value of maximum negative pressure is less than -100 Pa at the separation point of the incoming flow. $|C\bar{p}|$ increases as the blockage ratio increases. On the top slab of the box girder, $C\bar{p}$ is always negative, and the absolute value first decreases and then is in a plateau stage. On the downstream side, $|C\bar{p}|$ shows a decreasing trend. As the blockage ratio increases, $|C\bar{p}|$ decreases first and then an increasing trend can be found, which is the smallest at the 5% blockage ratio and the largest at the 10% blockage ratio.

At positive angles of attack, it can be clearly seen from Figs. 6(b) and 6(c) that the effect of the blockage ratio on the pressure distribution gradually increases with the increase of the angle of attack. The incoming flow is separated at the windward end, a strong negative pressure zone is formed and its size become larger with the increase of blockage ratio. The whole upper surface of the box girder is subjected to negative pressure and $C\bar{p}$ is always negative. As the blockage ratio increases, the area with pressure below -100 Pa gradually expands downstream and $|C\bar{p}|$ increases. On the lower surface of the box girder, the pressure distribution changes compared with that at 0° angle of attack. The pressure in most areas is positive and the positive pressure zone increases as the blockage ratio increases. The absolute value of pressure difference between upper and lower surfaces increases, which leads to the increase of C_L and C_M . At the windward end, $C\bar{p}$

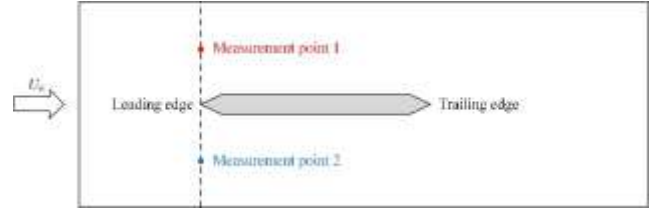


Fig. 9 Diagram of measurement points of wind speed

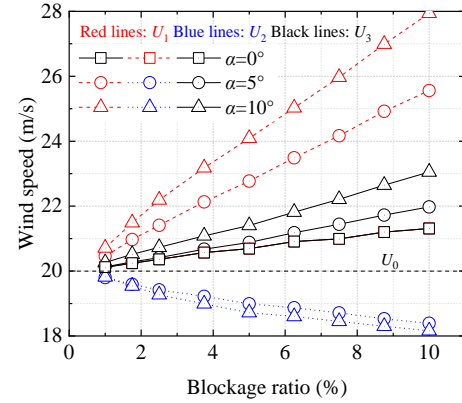


Fig. 10 Corrected wind speed versus blockage ratio

shows a trend of increasing first and then decreasing, changing its sign from positive to negative. The trend of pressure coefficient on the leeward side is similar to that at 0° angle of attack, but its absolute value increases obviously with the increase of the angle of attack.

In conclusion, the effect of blockage ratio on pressure distribution is considerable, which may be due to that the solid walls compresses the airflow on the upper and lower portions of the bridge model and restricts its expansion to the infinite region in the closed wind tunnel, resulting in the acceleration of airflow and the increase of $|C\bar{p}|$.

3.3 Aerodynamic coefficients correction by velocity around the girder

Then, the effect of blockage ratio on velocity around the box girder is investigated in this section. Because of the variation of the cross section of the wind tunnel, the wind speed around the box girder is not equal to that at the velocity-inlet. The wind speed at velocity-inlet is set as 20 m/s, Fig. 8 represents the contours of mean velocity of the stationary cross sections at different blockage ratios. It can be found that the mean wind speed near the box girder increases significantly with the increase of blockage ratio.

In the section model wind tunnel tests, the mean wind speed in the plane of leading edge is usually measured, probably at the mid-distance of between the wind tunnel wall and model, which can provide a partial correction for blockage effects. The diagram of measurement points of wind speed is shown in the Fig. 9, where U_0 is the wind speed at the velocity-inlet. The mean wind speeds at points 1 and 2 are defined as U_1 and U_2 respectively, and the average value of the two is U_3 .

The wind speed at velocity-inlet, i.e., U_0 , is 20m/s, and the wind speed at the measurement points at each blockage

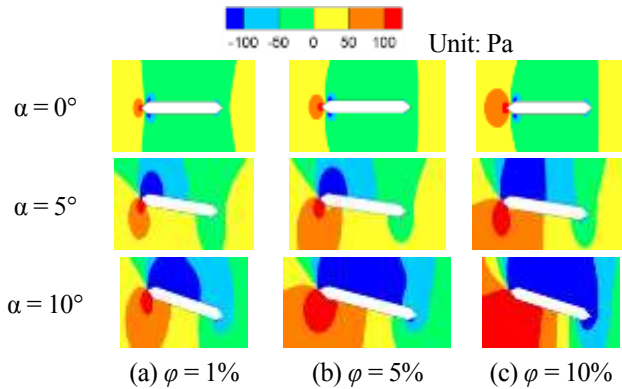


Fig. 7 Contours of statics pressure of the stationary cross sections for different blockage ratios

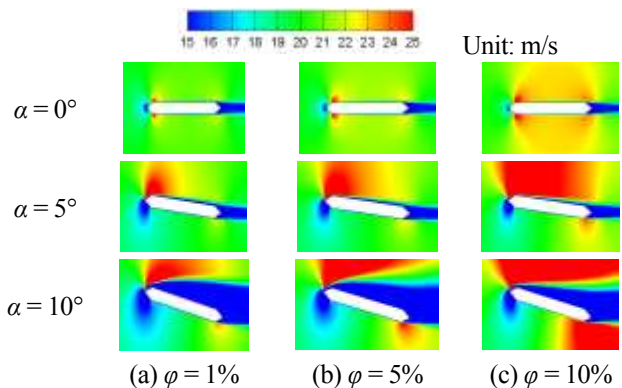


Fig. 8 Contours of mean velocity for different blockage ratios

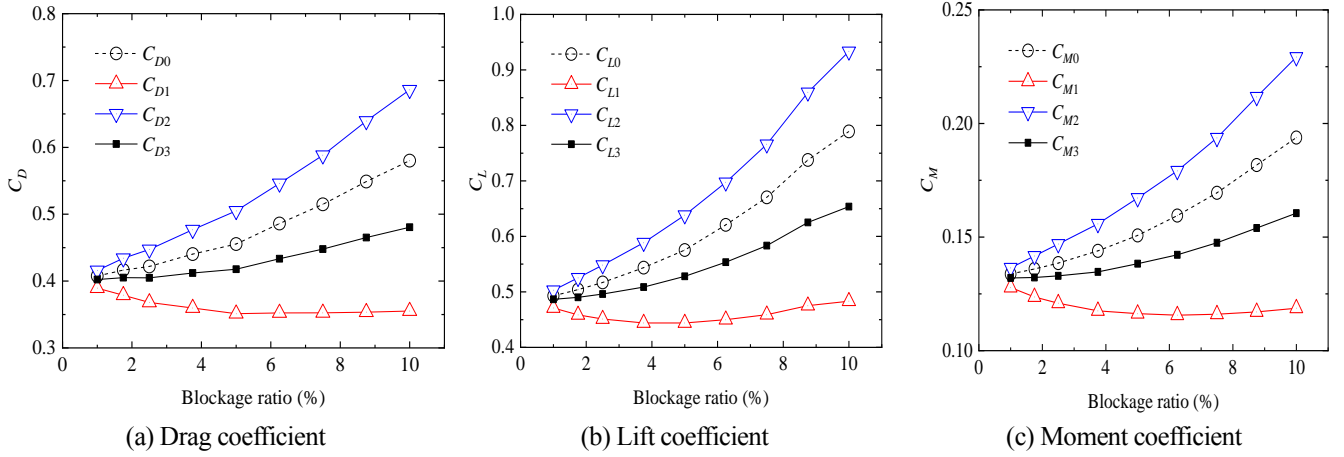


Fig. 11 Corrected mean aerodynamic coefficients at 5° angle of attack

ratio is shown in the Fig. 10. At 0° angle of attack, U_1 , U_2 and U_3 are equal at the same blockage ratio because the model is symmetrical. At +5° and +10° angles of attack, with the increase of blockage ratio, U_1 increases and U_2 decreases. However, the change range of U_1 is larger than that of U_2 , so the average value of the two, i.e., U_3 , increases as the increase of blockage ratio.

In order to compare the corrective effects of each corrected wind speed on aerodynamic coefficients, +5° angle of attack is taken as an example. The corrected aerodynamic coefficients calculated by substituting U_1 , U_2 and U_3 into Eqs. (1)-(3) are C_{i1} , C_{i2} and C_{i3} ($i = D, L, M$), respectively, as shown in Fig. 11. The aerodynamic coefficients calculated with different corrected wind speeds have little difference at low blockage ratio, i.e. $\varphi = 1\%$, but their difference increases as the increase of the blockage ratio. When the blockage ratio is the same, $C_{i2} > C_{i0} > C_{i3} > C_{i1}$. Based on the aerodynamic coefficients at $\varphi = 1\%$, the errors of aerodynamic coefficients at different blockage ratios are shown in the Table 1, where the cells filled with gray shadows represent no more than 10% error. Overall, when U_1 is used to correct the aerodynamic coefficients, the error of aerodynamic coefficients is the smallest, all within 10%. When U_3 is adopted for correction, the error is the smallest at low blockage ratio ($\varphi \leq 3.75\%$), but it will increase rapidly when the blockage ratio exceeds 5%. When the mean wind speed below the model, i.e., U_2 , is utilized for correction, the error is the largest and increases sharply as the increase of blockage ratio. When the blockage ratio is 10%, the errors of C_{D2} , C_{L2} and C_{M2} are 65.0%, 85.6% and 68.0%, respectively.

In conclusion, at 0° angle of attack, the correction effect is the same when the mean wind speed above or below the test model in the plane of leading edge is selected. In the case of positive angle of attack, it is the simplest and most effective to select the mean wind speed above the model to correct. But correspondingly, the mean wind speed below the model should be selected for correction at the negative angles of attack.

According to Scanlan's linearized theory, the self-excited forces of bridge are related to wind speed, so the blockage effect of wind speed will cause the blockage effect

of flutter performance and the change of flutter performance with blockage ratio needs further investigate.

4. Blockage effects of flutter performance

4.1 Flutter derivatives

Flutter derivative is the basis for calculating the critical flutter wind speed, which can be extracted by numerical simulation or wind tunnel test. The Scanlan's linearized theory of flutter derivatives is widely used to estimate the critical flutter speed. The self-excited lift force L_{se} and pitching moment M_{se} per unit length are defined as (R.H. Scanlan and Tomko 1971)

$$L_{se} = \frac{1}{2} \rho U^2 (2B) \left\{ KH_1^* \frac{\dot{h}}{U} + KH_2^* \frac{B\dot{\alpha}}{U} + K^2 H_3^* \alpha + K^2 H_4^* \frac{h}{B} \right\} \quad (4)$$

$$M_{se} = \frac{1}{2} \rho U^2 (2B^2) \left\{ KA_1^* \frac{\dot{h}}{U} + KA_2^* \frac{B\dot{\alpha}}{U} + K^2 A_3^* + K^2 A_4^* \frac{h}{B} \right\} \quad (5)$$

where ρ is the air density; $K = \omega B / U$ is the reduced frequency and ω is the circular frequency of vibration; h and α are the heaving and torsional displacements of the streamlined box girder respectively; H_i^* , A_i^* ($i = 1, 2, 3, 4$) are the flutter derivatives; and f is the vibration frequency. Single-degree-of-freedom (SDOF) harmonic vibration in heaving and torsion are imposed by user-defined function (UDF) respectively to extract flutter derivatives, and the center of the girder is set as the torsional center. The amplitude of the single peak is set as 0.0515B for heaving vibration, and 3° for torsional vibration. The frequencies of heaving and torsional vibration are both 2 Hz. According to the expression of self-excited force Eqs. (4)-(5), the corresponding flutter derivatives under different reduced wind speeds can be obtained by means of the least square method. The flutter derivatives of streamlined box girders at

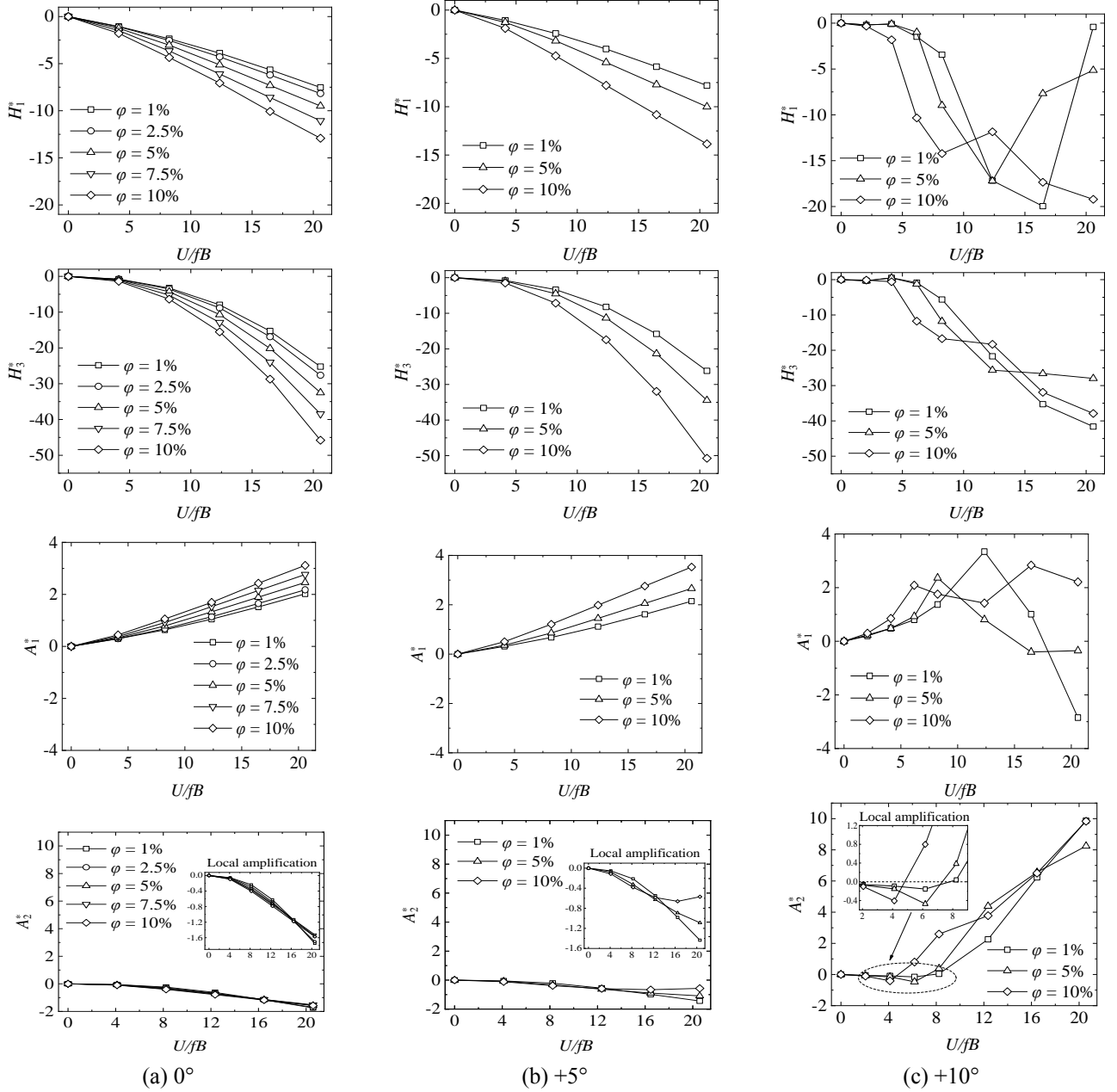


Fig. 12 Flutter derivatives of streamlined box girder under different blockage ratios

different blockage ratios are calculated respectively, common and large angles of attack are considered. Fig. 12 shows the direct flutter derivatives, H_1^* and A_2^* , and the coupled flutter derivatives, H_3^* and A_1^* . At 0° angle of attack, the box girder is a streamlined body, so both the values of A_2^* and H_1^* are always negative and decrease with the increase of U/fB , indicating that the uncoupled self-excited forces provide positive damping, which improves the stability of structural. The negative damping is mainly provided by the coupled term $H_3^*A_1^*$, and the absolute values of H_3^* and A_1^* increase with the increase of blockage ratio so that the flutter stability is reduced gradually. At $+5^\circ$ angle of attack, the variations of H_1^* , H_3^* and A_1^* are same as that at 0° angle of attack. But in the case of 10% blockage ratio, A_2^* has the trend of changing its sign from negative to positive with the increase of

reduced wind speed, indicating that the increase of blockage ratio aggravates the instability of cross section in torsional direction. At $+10^\circ$ angle of attack, the box girder exhibits the characteristics of a bluff body, the value of A_2^* changes its sign from negative to positive at each blockage ratio. As the increase of blockage ratio, the reduced wind speed corresponding to A_2^* changing to zero decreases, and the SDOF torsional flutter may occur due to the negative damping provided by uncoupled self-excited pitching moment. The phenomenon of H_1^* becoming positive also appears at large angle of attack, which reflects that the instability of heaving motion weakens.

4.2 Critical flutter state

To analyze the effects of blockage ratio on flutter

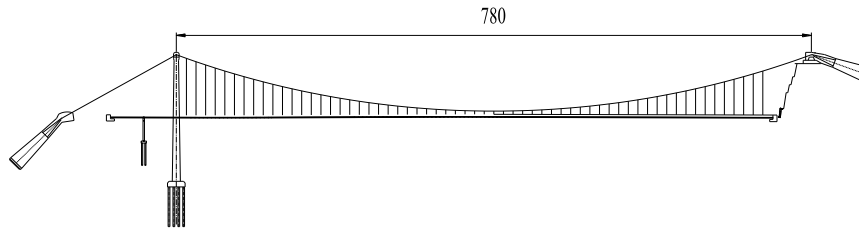


Fig. 13 Elevation of the suspension bridge (unit: m)

performance of long-span bridge with streamlined box girder, a realistic suspension bridge located in mountainous area is utilized to as an example. The elevation is shown in Fig. 13, and the main span is 780 m. The stiffening girder is a streamlined box girder with a width of 31.4 m and a height of 3 m. The mass and the mass moment of inertia per unit length are 2.30×10^4 kg/m and 3.02×10^6 kg·m²/m respectively. The three-dimensional (3D) finite element model is established by ANSYS software to analyze the dynamic characteristics of the bridge. The first order symmetric vertical and first order symmetric torsional frequencies of the bridge are 0.2043 Hz and 0.4613 Hz, respectively. The damping ratios of heaving and torsional vibration are both 0.5%.

Flutter derivatives obtained by the previous section are polynomial fitted, then the critical flutter wind speed and flutter frequency are calculated using a two degree-of-freedom flutter analysis method (Simiu and Scanlan 1996). Table 2 shows the critical flutter wind speeds and the flutter frequencies versus blockage ratios, and different angles of attack are still considered. At the same blockage ratio, the critical flutter wind speed decreases with the increase of attack angle, indicating that large angle of attack is a disadvantageous factor for the flutter performance of bridges. With the increase of blockage ratio, the critical flutter wind speed decreases at each angle of attack, and the flutter frequency shows an upward trend in general, which indicates that the proportion of torsional motion in flutter increases. The larger the angle of attack, the greater the effects of blockage ratio on flutter performance. The critical wind speed at 10% blockage ratio is 32.0%, 33.4% and 67.9% lower than that at 1% blockage ratio at 0°, +5° and +10° angle of attack, respectively. Therefore, when the

blockage ratio of wind tunnel test is too large to meet the requirements, the measured critical flutter wind speed will be far lower than the true value, especially at large angles of attack.

4.3 Flutter type analysis

Since torsional motion is involved in both bending-torsional coupled flutter and torsional flutter, the flutter type of box girder can be first analyzed by SDOF torsional motion. At 0° angle of attack, the reduced wind speed is taken as 12.98, which has exceeded the critical flutter wind speed at each blockage ratio, and Fig. 14 shows their contours of static pressure in one cycle T , where the times t , $t + 1/4T$, $t + 1/2T$, and $t + 3/4T$ correspond to the level position with the maximum clockwise torsional velocity (nose-upward), the maximum relative angle between the cross-section and the incoming wind, the level position with the maximum anti-clockwise torsional velocity (nose-downward), and the minimum relative angle, respectively. Fig. 15 shows the variation of the pressure difference between the upper and lower surfaces during the torsional motion of the box girder in one cycle, the abscissa is still the dimensionless parameter x^* (normalized by 0.5B), the pressure on upper surface is greater than that on lower surface is positive, and vice versa. Fig. 16. shows the time series of input energy by pitching moment in a torsion cycle at 1% blockage ratio versus angle of attack.

The following is mainly based on the 1% blockage ratio as an example for further analysis. Observing Figs. 14(a) and 15(a), the windward side pressure changes greatly while the leeward side pressure changes slightly during the vibration of the bridge girder, therefore, the aerodynamic characteristics of box girder is mainly controlled by the windward side. From t to $t + 1/4T$, the box girder moves clockwise, the pressure on the upper surface decreases and on the lower surface increases gradually, so the pressure difference on windward side between the upper and lower surfaces decreases gradually and changes its sign from positive to negative, which is negative for most of the time. Therefore, the pitching moment produces positive work, which is 0.67J (see Fig. 16). From $t + 1/4T$ to $t + 1/2T$, the main girder moves counterclockwise, the pressure on the upper surface increases and on the lower surface decreases.

The pressure difference between the upper and lower surfaces of the main girder increases gradually, but it is always negative, and the pitching moment produces negative work, which is -1.79J. From $t + 1/2T$ to $t + 3/4T$, the main girder continues to move counterclockwise, the pressure difference between the upper and lower surfaces

Table 2 Critical flutter state of the suspension bridge under different blockage ratios

Angle of attack	Blockage ratio				
	1%	2.5%	5%	7.5%	10%
Critical flutter wind speed (m/s)					
0°	129.7	123.2	110.2	98.7	88.2
+5°	121.3		102.7		80.8
+10°	71.4		58.8		22.9
Flutter frequency (Hz)					
0°	0.3451	0.3475	0.3584	0.3687	0.3773
+5°	0.3579		0.3666		0.3823
+10°	0.3731		0.3578		0.4271

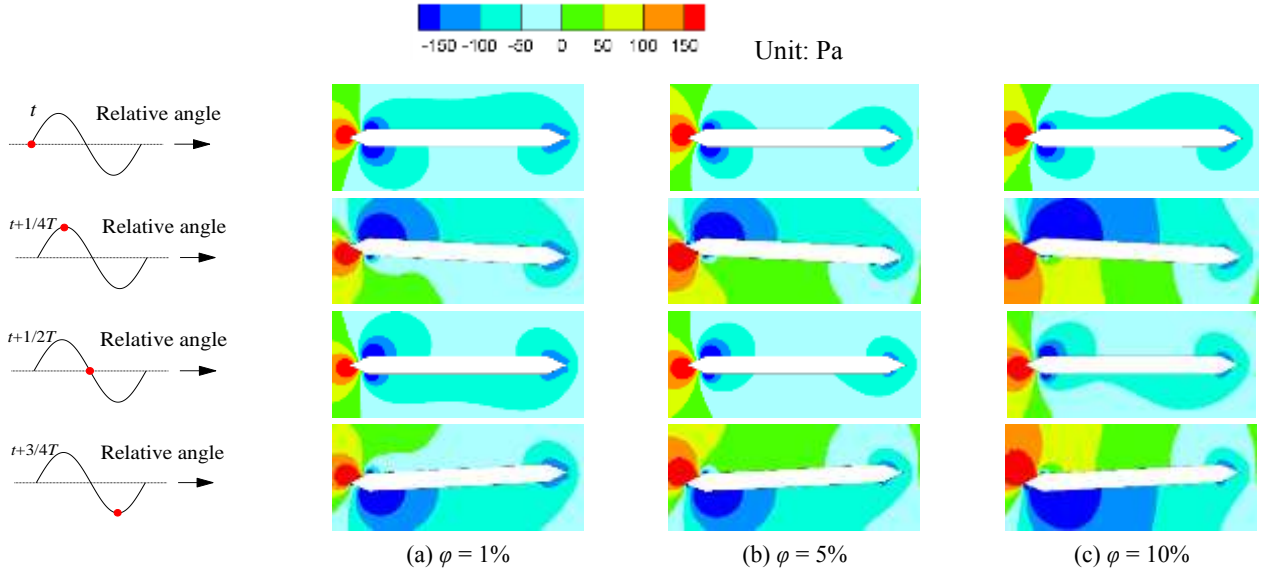


Fig. 14 Contours of statics pressure in one torsional cycle at 0° angle of attack

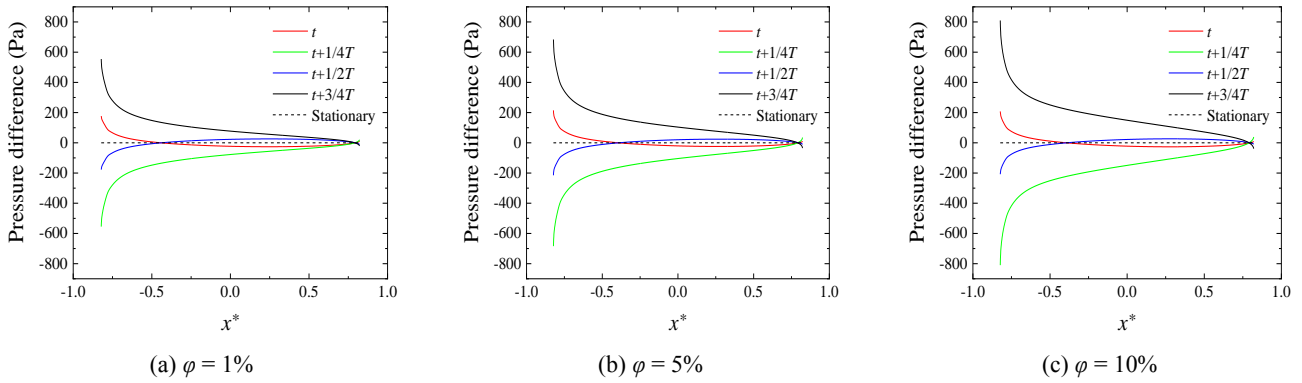


Fig. 15 Pressure difference on the surface of box girder in one torsional cycle at 0° angle of attack

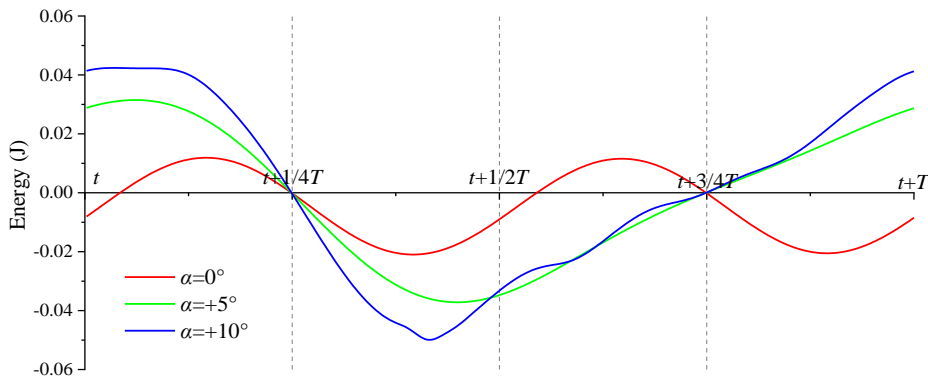


Fig. 16 Input energy by pitching moment in a torsion cycle at 1% blockage ratio

on the windward side increases further, and gradually changes its sign from negative to positive, which is positive for most of the time. Thus, the pitching moment produces positive work, which is 0.71J. From $t + 3/4T$ to $t + T$, the main girder moves clockwise, the pressure difference between the upper and lower surfaces of the main girder decreases gradually, but it is always positive, and the

pitching moment produces negative work, which is -1.83J. As the blockage ratio increases, the pressure difference between the upper and lower surfaces increases (see Fig. 15), so the input energy provided by pitching moment also decreases, as shown in the Table 3 which lists the input energy values versus reduced wind speed in a cycle of torsional vibration. With the increase of the reduced wind

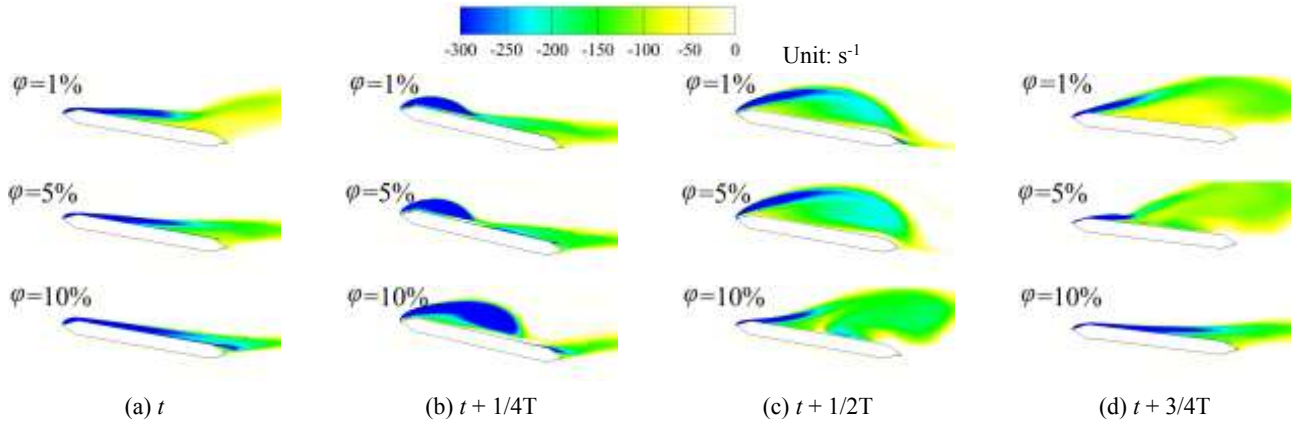


Fig. 17 Contours of instantaneous vorticity in one torsional cycle at $+10^\circ$ angle of attack

Table 3 Input energy by pitching moment in a torsion cycle (J)

Reduced wind speed	0° angle of attack			+5° angle of attack			+10° angle of attack		
	1%	5%	10%	1%	5%	10%	1%	5%	10%
2.06							-0.16	-0.32	-0.38
4.12							-0.36	-0.59	-1.48
6.18							-0.63	-1.37	+2.90
8.23	-0.85	-1.22	-1.46	-0.77	-1.17	-1.39	+0.14	+1.31	+9.59
12.35	-2.24	-2.60	-2.84	-2.00	-2.27	-2.13	+8.50	+16.41	+14.29
16.47	-4.16	-4.11	-4.26	-3.57	-3.21	-2.38			
20.58	-6.32	-5.64	-5.67	-5.22	-3.91	-2.19			

speed and far exceeding the flutter critical wind speed, the input energy decreases and its variation with the blockage ratio changes, but it is still less than 0, indicating that the structure cannot maintain the existing vibration, that is, the flutter type is coupled bending-torsional flutter rather than torsional flutter.

The input energy decreases gradually with the increase of attack angle. At $+10^\circ$ angle of attack, the input energy changes its sign from negative to positive as the increase of the reduced wind speed (see Table 3), which indicates that the torsional vibration of the structure is unstable and torsional flutter may occur. The larger the blockage ratio, the lower the reduced wind speed corresponding to the change of input energy from negative to positive, which is consistent with the variation of flutter derivative A_2^* . This phenomenon can be explained by the contours of instantaneous vorticity in one torsional cycle (see Fig. 17), and the reduced wind speed is taken as 8.23. The cross section rotates clockwise from t to $t + 1/4T$ during which a big vortex is formed on the windward side and excites the clockwise rotation.

4.4 Critical flutter wind speed correction

From the results of the previous section, it can be seen that the effects of blockage ratio on the flutter performance of bridge cannot be ignored. In Section 3.3, the aerodynamic coefficients can be corrected by the mean

wind speed in the plane of the leading edge of the bridge model in wind tunnel test, which can reduce the error better. In this section, the critical flutter wind speed is corrected by the same method, taking 0° angle of attack as an example. Some important corrected flutter derivatives are shown in Fig. 18. At the same blockage ratio, the change of A_2^* is very small, while the absolute values of H_3^* and A_1^* decrease slightly, so the negative damping provided by the coupled term $H_3^*A_1^*$ decreases. The corrected critical flutter wind speed and the flutter frequency are shown in the Fig. 19. The critical flutter wind speed and the flutter frequency after correction differ little from those before correction, and the change trend is the same. The error of the corrected critical wind speed is still very large at high blockage ratio, up to 27.5% at $\varphi = 10\%$. It can be seen that the effect of correcting the critical flutter wind speed by the mean wind speed in the plane of the bridge model is very limited. This may be due to the fact that flutter is a complex dynamic response which is affected by many factors, unlike static conditions, so it is not enough to correct it only from one aspect.

As a consequence, when the test conditions are limited and the low blockage ratio cannot be guaranteed, it is necessary to correct the measured critical flutter wind speed by fitting formula. Based on the critical flutter wind speeds at different blockage ratios, a curve is constituted using quadratic polynomial fitting method, expressed as the following equation

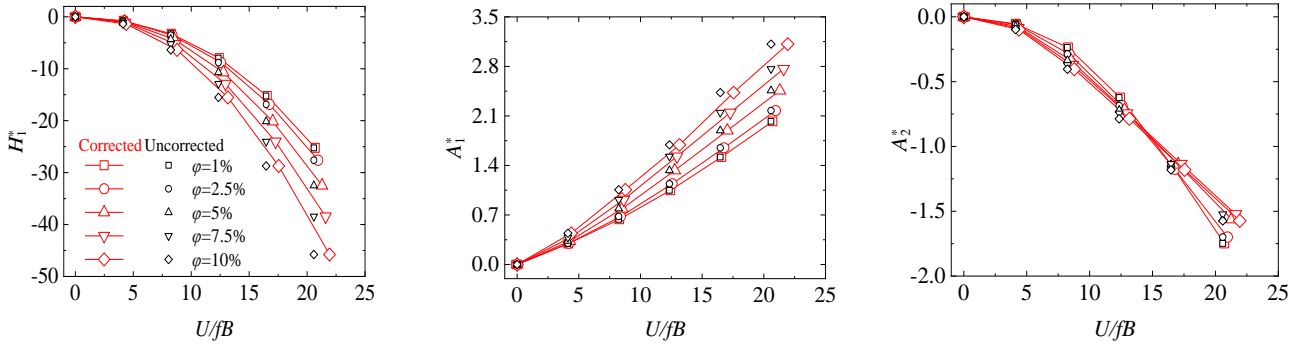


Fig. 18 Corrected flutter derivatives at 0° angle of attack

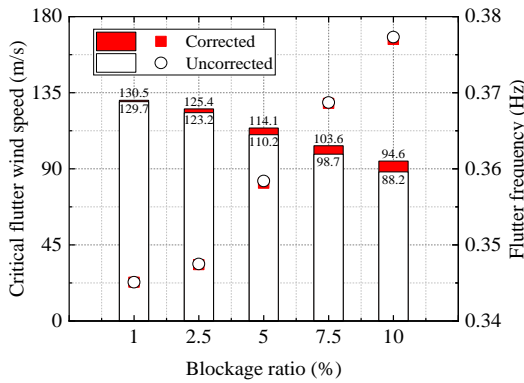


Fig. 19 Corrected critical flutter state at 0° angle of attack

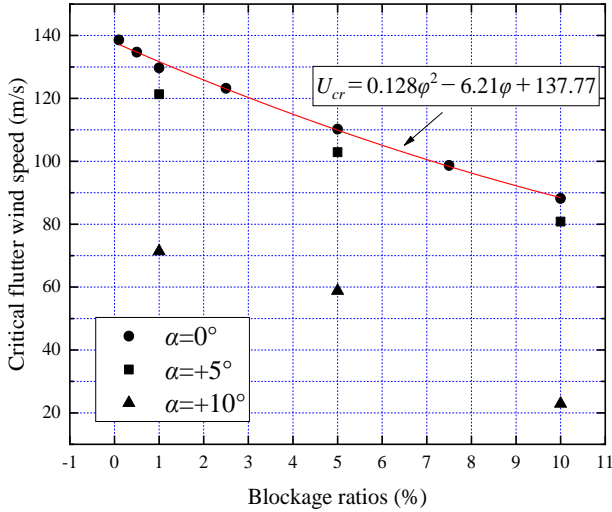


Fig. 20 Variation curve of critical flutter wind speed with blockage ratio

$$U_{cr} = 0.128\phi^2 - 6.21\phi + 137.77 \quad (6)$$

as shown in Fig. 20. This curve can accurately reflect the change of critical flutter wind speed as blockage ratio at 0° angle of attack, and at large angles of attack, although the value of critical wind speed decreases, its variation trend with blockage ratio is similar to that at 0° angle of attack and the slope is approximately equal.

With the increase of the blockage ratio, the critical flutter wind speed of the streamlined box girder is more

obviously affected by the boundary effect, the difference between the real results and measured results is larger. Therefore, in the analysis of flutter performance of streamlined box girder, the blockage ratio should be reduced as far as possible. It is recommended that the blockage ratio should be controlled within 2.5%. If the test and calculation conditions are limited and the blockage ratio cannot be controlled within 2.5%, the results can be corrected by Eq. (6).

5. Conclusion

In the present paper, important aspects, including aerodynamic coefficients, pressure distributions, velocity around the girder, flutter derivatives, critical flutter state, are considered to explore the blockage effects of a streamlined box girder on the aerodynamic characteristics and flutter performance. Based on the results of CFD simulations, the following conclusions are made:

- The aerodynamic coefficients of the streamlined box girder show significant blockage effects. The drag coefficient, lift coefficient and moment coefficient increase as the increase of the blockage ratio, and the larger the angle of attack, the more obvious the blockage effect. At positive angles of attack, the aerodynamic coefficients can be corrected by the mean wind speed above the bridge model in the plane of leading edge, which can reduce the error better.
- The effects of the blockage ratio on the pressure distribution of the box girder are more obvious with the increase of the angle of attack. At positive angles of attack, the incoming stream is separated at the windward end, a negative pressure zone is formed on the upper surface and its size become larger with the increase of blockage ratio. On the lower surface of the box girder, the pressure in most areas is positive and expands as the blockage ratio increases, so the absolute value of pressure difference between upper and lower surfaces increases, which leads to the increase of C_L and C_M . The solid wall compresses the airflow on the upper and lower portions of the bridge model and restricts its expansion to the infinite region in the closed wind tunnel, so the mean

wind speed near the box girder increases significantly.

- The change of the blockage ratio has great effects on the flutter performance of the streamlined box girder. At each angle of attack, the critical flutter wind speed decreases as the blockage ratio increases. At lower angles of attack, the box girder is a streamlined body, the uncoupled self-excited forces provide positive damping, the input energy provided by the pitching moment decreases as the increase of the reduced wind speed and is always negative at all blockage ratios, leading to bending-torsion coupling flutter. At larger angles of attack, the box girder more like a bluff body, the uncoupled self-excited pitching moment produces negative damping, the input energy changes its sign from negative to positive as the increase of the reduced wind speed, the movement of vortex formed at the windward side to the leeward side is the main reason for the torsional flutter of the bridge. The increase of blockage ratio aggravates the instability of cross-section in torsional direction, so the critical flutter wind speed decreases.
- In the wind tunnel test of streamlined box girder, it is recommended that the blockage ratio be controlled within 2.5%. When the blockage ratio is too large, the effect of correcting the critical flutter wind speed by the mean wind speed in the plane of the leading edge of model is very limited. And the correction equation of critical flutter wind speed for streamlined box girder at 0° angle of attack is given, which can provide reference for wind resistance design of streamlined box girders in practical engineering.

Acknowledgments

The research described in this paper was financially supported by the Natural Science Foundation of China (Grants 51708463, 51525804) and the Fundamental Research Funds for the Central Universities (2682019CX04).

References

- Cheng, H.M. (2003), *Wind Tunnel Experiment Interference and Correction*. National Defense Industry Press, Beijing, China.
- Ge, Y.J., Zou, X.J. and Yang, Y.X. (2009), "Aerodynamic stabilization of central stabilizers for box girder suspension bridges", *Wind Struct., Int. J.*, **12**(4), 285-298. <https://doi.org/10.12989/was.2009.12.4.285>
- Ge, Y.J. and Xiang, H.F. (2008), "Recent development of bridge aerodynamics in China", *J Wind Eng. Ind. Aerodyn.*, **96**(6), 736-768. <https://doi.org/10.1016/j.jweia.2007.06.045>.
- Gu, M. and Huang, J. (2016), "Research Progress of Wind Tunnel Blockage Effects on Building Models", *J. Tongji Univ. Nat. Sci.*, **44**(1), 1-10.
- He, X.H., Li, H., Wang, H.F., Fang, D.X. and Liu, M.T. (2017), "Effects of geometrical parameters on the aerodynamic characteristics of a streamlined flat box girder", *J. Wind Eng. Ind. Aerodyn.*, **170**, 56-67. <https://doi.org/10.1016/j.jweia.2017.08.009>.
- Huang, J. and Gu, M. (2015), "Experimental investigation of blockage effects on mean pressure of rectangular tall buildings in the wind tunnel", *Acta Aerodyn. Sin.*, **33**(3).
- Huang, L., Liao, H.L., Wang, B. and Li, Y.L. (2009), "Numerical simulation for aerodynamic derivatives of bridge deck", *Simul. Model. Pract. Theory.*, **17**(4), 719-729. <https://doi.org/10.1016/j.simpat.2008.12.004>
- Hunt, A. (1982), "Wind-tunnel measurements of surface pressures on cubic building models at several scales", *J. Wind Eng. Ind. Aerodyn.*, **10**(2), 137-163. [https://doi.org/10.1016/0167-6105\(82\)90061-7](https://doi.org/10.1016/0167-6105(82)90061-7).
- Ito, Y., Shirato, H. and Matsumoto, M. (2014), "Coherence characteristics of fluctuating lift forces for rectangular shape with various fairing decks", *J. Wind Eng. Ind. Aerodyn.*, **135**, 34-45. <https://doi.org/10.1016/j.jweia.2014.10.003>
- Kubo, Y., Miyazaki, M. and Kato, K. (1989), "Effects of end plates and blockage of structural members on drag forces", *J. Wind Eng. Ind. Aerodyn.*, **32**(3), 329-342. [https://doi.org/10.1016/0167-6105\(89\)90006-8](https://doi.org/10.1016/0167-6105(89)90006-8).
- Larsen, A. (2000), "Aerodynamics of the Tacoma Narrows Bridge - 60 Years Later", *Struct. Eng. Int.*, **10**(4), 243-248.
- Larsen, A. (1993), "Aerodynamic aspects of the final design of the 1624 m suspension bridge across the Great Belt", *J. Wind Eng. Ind. Aerodyn.*, **48**(2), 261-285.
- Larsen, A., Savage, M., Lafrenière, A., Hui, M.C.H. and Larsen, S.V. (2008), "Investigation of vortex response of a twin box bridge section at high and low Reynolds numbers", *J. Wind Eng. Ind. Aerodyn.*, **96**(6), 934-944. <https://doi.org/10.1016/j.jweia.2007.06.020>.
- Larsen, A. and Wall, A. (2012), "Shaping of bridge box girders to avoid vortex shedding response", *J. Wind Eng. Ind. Aerodyn.*, **104-106**, 159-165. <https://doi.org/10.1016/j.jweia.2012.04.018>.
- Li, Y.L., Chen, X.Y., Wang, B. and Zhu, L.D. (2018), "Blockage-effects and amplitude conversion of vortex-induced-vibration for flat-box girder", *Eng. Mech.*, **35**(11), 45-78.
- Ma, C.M., Duan, Q.S. and Liao, H.L. (2018), "Experimental Investigation on Aerodynamic Behavior of a Long Span Cable-stayed Bridge Under Construction", *KSCE J. Civ. Eng.*, **22**(7), 2492-2501.
- Miranda, S., Patruno, L., Ricci, M. and Ubertini, F. (2015), "Numerical study of a twin box bridge deck with increasing gap ratio by using RANS and LES approaches", *Eng. Struct.*, **99**, 546-558. <https://doi.org/10.1016/j.engstruct.2015.05.017>.
- Scanlan, R.H. and Tomko, J.J. (1971), "Airfoil and Bridge Deck Flutter Derivatives", *J. Eng. Mech. Div.*, **97**(6), 1717-1737.
- Simiu, E. and Scanlan, R.H. (1996), *Wind effects on structures: fundamentals and applications to design*, (3rd Edition), John Wiley, New York, NY, USA.
- Sukamta, Nagao, F., Noda, M. and Muneta, K. (2008), "Aerodynamic stabilizing mechanism of a cable stayed bridge with two edge box girder", *The Proceedings of 6th International Colloquium on: Bluff Bodies Aerodynamics & Applications*, Milano, Italy, July.
- Takeda, K. and Kato, M. (1992), "Wind tunnel blockage effects on drag coefficient and wind-induced vibration", *J. Wind Eng. Ind. Aerodyn.*, **42**(1), 897-908. [https://doi.org/10.1016/0167-6105\(92\)90096-S](https://doi.org/10.1016/0167-6105(92)90096-S).
- Tang, H.J., Li, Y.L. and Shum, K. (2018), "Flutter performance and aerodynamic mechanism of plate with central stabilizer at large angles of attack", *Adv. Struct. Eng.*, **21**(3), 335-346. <https://doi.org/10.1177/1369433217717120>.
- Theodorsen, T. (1935), *General theory of aerodynamic instability and the mechanism of flutter*, National Advisory Committee for Aeronautics, Washington, DC, USA.
- Walther, J.H. (1994), "Discrete Vortex Method for Two-

- dimensional Flow past Bodies of Arbitrary Shape Undergoing Prescribed Rotary and Translational Motion”, Ph.D. Dissertation, Technical University of Denmark, Copenhagen.
- Zhou, Z.Y., Yang, T., Ding, Q.S. and Ge, Y.J. (2015), “Mechanism on suppression in vortex-induced vibration of bridge deck with long projecting slab with countermeasures”, *Wind Struct., Int. J.*, **20**(5), 643-660. <https://doi.org/10.12989/was.2015.20.5.643>.
- Zhu, L.D., Meng, X.L. and Guo, Z.S. (2013), “Nonlinear mathematical model of vortex-induced vertical force on a flat closed-box bridge deck”, *J. Wind Eng. Ind. Aerodyn.*, **122**, 69-82. <https://doi.org/10.1016/j.jweia.2013.07.008>.
- Zhu, Z.W. and Chen, Z.Q. (2004), “Numerical simulations for aerodynamic derivatives and critical flutter velocity of bridge deck”, *China J. Highw. Transp.*, **17**(3), 41-45.

AD